



A calibration of the Belle II hadronic tag-side reconstruction algorithm with $B \rightarrow X\ell\nu$ decays

F. Abudinén,⁴⁷ I. Adachi,^{24,21} R. Adak,¹⁸ K. Adamczyk,⁷² P. Ahlburg,¹⁰⁹ J. K. Ahn,⁵⁴
H. Aihara,¹²⁷ N. Akopov,¹³³ A. Aloisio,^{97,40} F. Ameli,⁴⁴ L. Andricek,⁶³ N. Anh Ky,^{37,14}
D. M. Asner,³ H. Atmacan,¹¹¹ V. Aulchenko,^{4,74} T. Aushev,²⁶ V. Aushev,⁸⁸ T. Aziz,⁸⁹
V. Babu,¹² S. Bacher,⁷² S. Baehr,⁵¹ S. Bahinipati,²⁸ A. M. Bakich,¹²⁶ P. Bambade,¹⁰⁶
Sw. Banerjee,¹¹⁶ S. Bansal,⁷⁹ M. Barrett,²⁴ G. Batignani,^{100,43} J. Baudot,¹⁰⁷
A. Beaulieu,¹²⁹ J. Becker,⁵¹ P. K. Behera,³¹ M. Bender,⁵⁹ J. V. Bennett,¹²⁰ E. Bernieri,⁴⁵
F. U. Bernlochner,¹⁰⁹ M. Bertemes,³⁴ M. Bessner,¹¹³ S. Bettarini,^{100,43} V. Bhardwaj,²⁷
B. Bhuyan,²⁹ F. Bianchi,^{103,46} T. Bilka,⁷ S. Bilokin,⁵⁹ D. Biswas,¹¹⁶ A. Bobrov,^{4,74}
A. Bondar,^{4,74} G. Bonvicini,¹³¹ A. Bozek,⁷² M. Bračko,^{118,87} P. Branchini,⁴⁵ N. Braun,⁵¹
R. A. Briere,⁵ T. E. Browder,¹¹³ D. N. Brown,¹¹⁶ A. Budano,⁴⁵ L. Burmistrov,¹⁰⁶
S. Bussino,^{102,45} M. Campajola,^{97,40} L. Cao,¹⁰⁹ G. Caria,¹¹⁹ G. Casarosa,^{100,43}
C. Cecchi,^{99,42} D. Červenkov,⁷ M.-C. Chang,¹⁷ P. Chang,⁷⁰ R. Cheaib,¹¹⁰ V. Chekelian,⁶²
Y. Q. Chen,¹²³ Y.-T. Chen,⁷⁰ B. G. Cheon,²³ K. Chilikin,⁵⁷ K. Chirapatpimol,⁸
H.-E. Cho,²³ K. Cho,⁵³ S.-J. Cho,¹³⁴ S.-K. Choi,²² S. Choudhury,³⁰ D. Cinabro,¹³¹
L. Corona,^{100,43} L. M. Cremaldi,¹²⁰ D. Cuesta,¹⁰⁷ S. Cunliffe,¹² T. Czank,¹²⁸ N. Dash,³¹
F. Dattola,¹² E. De La Cruz-Burelo,⁶ G. De Nardo,^{97,40} M. De Nuccio,¹² G. De Pietro,⁴⁵
R. de Sangro,³⁹ B. Deschamps,¹⁰⁹ M. Destefanis,^{103,46} S. Dey,⁹¹ A. De Yta-Hernandez,⁶
A. Di Canto,³ F. Di Capua,^{97,40} S. Di Carlo,¹⁰⁶ J. Dingfelder,¹⁰⁹ Z. Doležal,⁷
I. Domínguez Jiménez,⁹⁶ T. V. Dong,¹⁸ K. Dort,⁵⁰ D. Dossett,¹¹⁹ S. Dubey,¹¹³ S. Duell,¹⁰⁹
G. Dujany,¹⁰⁷ S. Eidelman,^{4,57,74} M. Eliachevitch,¹⁰⁹ D. Epifanov,^{4,74} J. E. Fast,⁷⁸
T. Ferber,¹² D. Ferlewicz,¹¹⁹ G. Finocchiaro,³⁹ S. Fiore,⁴⁴ P. Fischer,¹¹⁴ A. Fodor,⁶⁴
F. Forti,^{100,43} A. Frey,¹⁹ M. Friedl,³⁴ B. G. Fulson,⁷⁸ M. Gabriel,⁶² N. Gabyshev,^{4,74}
E. Ganiev,^{104,47} M. Garcia-Hernandez,⁶ R. Garg,⁷⁹ A. Garmash,^{4,74} V. Gaur,¹³⁰
A. Gaz,^{66,67} U. Gebauer,¹⁹ M. Gelb,⁵¹ A. Gellrich,¹² J. Gemmler,⁵¹ T. Geßler,⁵⁰
D. Getzkow,⁵⁰ R. Giordano,^{97,40} A. Giri,³⁰ A. Glazov,¹² B. Gobbo,⁴⁷ R. Godang,¹²⁴
P. Goldenzweig,⁵¹ B. Golob,^{115,87} P. Gomis,³⁸ P. Grace,¹⁰⁸ W. Gradl,⁴⁹ E. Graziani,⁴⁵
D. Greenwald,⁹⁰ Y. Guan,¹¹¹ C. Hadjivasiliou,⁷⁸ S. Halder,⁸⁹ K. Hara,^{24,21} T. Hara,^{24,21}
O. Hartbrich,¹¹³ T. Hauth,⁵¹ K. Hayasaka,⁷³ H. Hayashii,⁶⁹ C. Hearty,^{110,36} M. Heck,⁵¹
M. T. Hedges,¹¹³ I. Heredia de la Cruz,^{6,11} M. Hernández Villanueva,¹²⁰ A. Hershenhorn,¹¹⁰
T. Higuchi,¹²⁸ E. C. Hill,¹¹⁰ H. Hirata,⁶⁶ M. Hoek,⁴⁹ M. Hohmann,¹¹⁹ S. Hollitt,¹⁰⁸
T. Hotta,⁷⁷ C.-L. Hsu,¹²⁶ Y. Hu,³⁵ K. Huang,⁷⁰ T. Iijima,^{66,67} K. Inami,⁶⁶ G. Inguglia,³⁴
J. Irakkathil Jabbar,⁵¹ A. Ishikawa,^{24,21} R. Itoh,^{24,21} M. Iwasaki,⁷⁶ Y. Iwasaki,²⁴
S. Iwata,⁹⁵ P. Jackson,¹⁰⁸ W. W. Jacobs,³² I. Jaegle,¹¹² D. E. Jaffe,³ E.-J. Jang,²²
M. Jeandron,¹²⁰ H. B. Jeon,⁵⁶ S. Jia,¹⁸ Y. Jin,⁴⁷ C. Joo,¹²⁸ K. K. Joo,¹⁰ I. Kadenko,⁸⁸
J. Kahn,⁵¹ H. Kakuno,⁹⁵ A. B. Kaliyar,⁸⁹ J. Kandra,⁷ K. H. Kang,⁵⁶ P. Kapusta,⁷²

42 R. Karl,¹² G. Karyan,¹³³ Y. Kato,^{66,67} H. Kawai,⁹ T. Kawasaki,⁵² T. Keck,⁵¹
 43 C. Ketter,¹¹³ H. Kichimi,²⁴ C. Kiesling,⁶² B. H. Kim,⁸³ C.-H. Kim,²³ D. Y. Kim,⁸⁶
 44 H. J. Kim,⁵⁶ J. B. Kim,⁵⁴ K.-H. Kim,¹³⁴ K. Kim,⁵⁴ S.-H. Kim,⁸³ Y.-K. Kim,¹³⁴
 45 Y. Kim,⁵⁴ T. D. Kimmel,¹³⁰ H. Kindo,^{24,21} K. Kinoshita,¹¹¹ B. Kirby,³ C. Kleinwort,¹²
 46 B. Knysh,¹⁰⁶ P. Kodyš,⁷ T. Koga,²⁴ S. Kohani,¹¹³ I. Komarov,¹² T. Konno,⁵²
 47 S. Korpar,^{118,87} N. Kovalchuk,¹² T. M. G. Kraetzschmar,⁶² P. Križan,^{115,87} R. Kroeger,¹²⁰
 48 J. F. Krohn,¹¹⁹ P. Krokovny,^{4,74} H. Krüger,¹⁰⁹ W. Kuehn,⁵⁰ T. Kuhr,⁵⁹ J. Kumar,⁵
 49 M. Kumar,⁶¹ R. Kumar,⁸¹ K. Kumara,¹³¹ T. Kumita,⁹⁵ T. Kunigo,²⁴ M. Künzel,^{12,59}
 50 S. Kurz,¹² A. Kuzmin,^{4,74} P. Kvasnička,⁷ Y.-J. Kwon,¹³⁴ S. Lacaprara,⁴¹ Y.-T. Lai,¹²⁸
 51 C. La Licata,¹²⁸ K. Lalwani,⁶¹ L. Lanceri,⁴⁷ J. S. Lange,⁵⁰ K. Lautenbach,⁵⁰ P. J. Laycock,³
 52 F. R. Le Diberder,¹⁰⁶ I.-S. Lee,²³ S. C. Lee,⁵⁶ P. Leitl,⁶² D. Levit,⁹⁰ P. M. Lewis,¹⁰⁹ C. Li,⁵⁸
 53 L. K. Li,¹¹¹ S. X. Li,² Y. M. Li,³⁵ Y. B. Li,⁸⁰ J. Libby,³¹ K. Lieret,⁵⁹ L. Li Gioi,⁶² J. Lin,⁷⁰
 54 Z. Liptak,¹¹³ Q. Y. Liu,¹² Z. A. Liu,³⁵ D. Liventsev,^{131,24} S. Longo,¹² A. Loos,¹²⁵ P. Lu,⁷⁰
 55 M. Lubej,⁸⁷ T. Lueck,⁵⁹ F. Luetticke,¹⁰⁹ T. Luo,¹⁸ C. MacQueen,¹¹⁹ Y. Maeda,^{66,67}
 56 M. Maggiora,^{103,46} S. Maity,²⁸ R. Manfredi,^{104,47} E. Manoni,⁴² S. Marcello,^{103,46}
 57 C. Marinas,³⁸ A. Martini,^{102,45} M. Masuda,^{15,77} T. Matsuda,¹²¹ K. Matsuoka,^{66,67}
 58 D. Matvienko,^{4,57,74} J. McNeil,¹¹² F. Meggendorfer,⁶² J. C. Mei,¹⁸ F. Meier,¹³
 59 M. Merola,^{97,40} F. Metzner,⁵¹ M. Milesi,¹¹⁹ C. Miller,¹²⁹ K. Miyabayashi,⁶⁹ H. Miyake,^{24,21}
 60 H. Miyata,⁷³ R. Mizuk,^{57,26} K. Azmi,¹¹⁷ G. B. Mohanty,⁸⁹ H. Moon,⁵⁴ T. Moon,⁸³
 61 J. A. Mora Grimaldo,¹²⁷ A. Morda,⁴¹ T. Morii,¹²⁸ H.-G. Moser,⁶² M. Mrvar,³⁴
 62 F. Mueller,⁶² F. J. Müller,¹² Th. Muller,⁵¹ G. Muroyama,⁶⁶ C. Murphy,¹²⁸ R. Mussa,⁴⁶
 63 K. Nakagiri,²⁴ I. Nakamura,^{24,21} K. R. Nakamura,^{24,21} E. Nakano,⁷⁶ M. Nakao,^{24,21}
 64 H. Nakayama,^{24,21} H. Nakazawa,⁷⁰ T. Nanut,⁸⁷ Z. Natkaniec,⁷² A. Natochii,¹¹³
 65 M. Nayak,⁹¹ G. Nazaryan,¹³³ D. Neverov,⁶⁶ C. Niebuhr,¹² M. Niiyama,⁵⁵ J. Ninkovic,⁶³
 66 N. K. Nisar,³ S. Nishida,^{24,21} K. Nishimura,¹¹³ M. Nishimura,²⁴ M. H. A. Nouxman,¹¹⁷
 67 B. Oberhof,³⁹ K. Ogawa,⁷³ S. Ogawa,⁹² S. L. Olsen,²² Y. Onishchuk,⁸⁸ H. Ono,⁷³
 68 Y. Onuki,¹²⁷ P. Oskin,⁵⁷ E. R. Oxford,⁵ H. Ozaki,^{24,21} P. Pakhlov,^{57,65} G. Pakhlova,^{26,57}
 69 A. Paladino,^{100,43} T. Pang,¹²² A. Panta,¹²⁰ E. Paoloni,^{100,43} S. Pardi,⁴⁰ C. Park,¹³⁴
 70 H. Park,⁵⁶ S.-H. Park,¹³⁴ B. Paschen,¹⁰⁹ A. Passeri,⁴⁵ A. Pathak,¹¹⁶ S. Patra,²⁷
 71 S. Paul,⁹⁰ T. K. Pedlar,⁶⁰ I. Peruzzi,³⁹ R. Peschke,¹¹³ R. Pestotnik,⁸⁷ M. Piccolo,³⁹
 72 L. E. Pilonen,¹³⁰ P. L. M. Podesta-Lerma,⁹⁶ G. Polat,¹ V. Popov,²⁶ C. Praz,¹²
 73 E. Prencipe,¹⁶ M. T. Prim,¹⁰⁹ M. V. Purohit,⁷⁵ N. Rad,¹² P. Rados,¹² R. Rasheed,¹⁰⁷
 74 M. Reif,⁶² S. Reiter,⁵⁰ M. Remnev,^{4,74} P. K. Resmi,³¹ I. Ripp-Baudot,¹⁰⁷ M. Ritter,⁵⁹
 75 M. Ritzert,¹¹⁴ G. Rizzo,^{100,43} L. B. Rizzuto,⁸⁷ S. H. Robertson,^{64,36} D. Rodríguez Pérez,⁹⁶
 76 J. M. Roney,^{129,36} C. Rosenfeld,¹²⁵ A. Rostomyan,¹² N. Rout,³¹ M. Rozanska,⁷²
 77 G. Russo,^{97,40} D. Sahoo,⁸⁹ Y. Sakai,^{24,21} D. A. Sanders,¹²⁰ S. Sandilya,¹¹¹ A. Sangal,¹¹¹
 78 L. Santelj,^{115,87} P. Sartori,^{98,41} J. Sasaki,¹²⁷ Y. Sato,⁹³ V. Savinov,¹²² B. Scavino,⁴⁹
 79 M. Schram,⁷⁸ H. Schreeck,¹⁹ J. Schueler,¹¹³ C. Schwanda,³⁴ A. J. Schwartz,¹¹¹
 80 B. Schwenker,¹⁹ R. M. Seddon,⁶⁴ Y. Seino,⁷³ A. Selce,^{101,44} K. Senyo,¹³² I. S. Seong,¹¹³
 81 J. Serrano,¹ M. E. Sevier,¹¹⁹ C. Sfienti,⁴⁹ V. Shebalin,¹¹³ C. P. Shen,² H. Shibuya,⁹²
 82 J.-G. Shiu,⁷⁰ B. Shwartz,^{4,74} A. Sibidanov,¹²⁹ F. Simon,⁶² J. B. Singh,⁷⁹ S. Skambraks,⁶²
 83 K. Smith,¹¹⁹ R. J. Sobie,^{129,36} A. Soffer,⁹¹ A. Sokolov,³³ Y. Soloviev,¹² E. Solovieva,⁵⁷
 84 S. Spataro,^{103,46} B. Spruck,⁴⁹ M. Starič,⁸⁷ S. Stefkova,¹² Z. S. Stottler,¹³⁰ R. Stroili,^{98,41}
 85 J. Strube,⁷⁸ J. Stypula,⁷² M. Sumihama,^{20,77} K. Sumisawa,^{24,21} T. Sumiyoshi,⁹⁵

86 D. J. Summers,¹²⁰ W. Sutcliffe,¹⁰⁹ K. Suzuki,⁶⁶ S. Y. Suzuki,^{24,21} H. Svidras,¹² M. Tabata,⁹
87 M. Takahashi,¹² M. Takizawa,^{82,25,84} U. Tamponi,⁴⁶ S. Tanaka,^{24,21} K. Tanida,⁴⁸
88 H. Tanigawa,¹²⁷ N. Taniguchi,²⁴ Y. Tao,¹¹² P. Taras,¹⁰⁵ F. Tenchini,¹² D. Tonelli,⁴⁷
89 E. Torassa,⁴¹ K. Trabelsi,¹⁰⁶ T. Tsuboyama,^{24,21} N. Tsuzuki,⁶⁶ M. Uchida,⁹⁴ I. Ueda,^{24,21}
90 S. Uehara,^{24,21} T. Ueno,⁹³ T. Uglov,^{57,26} K. Unger,⁵¹ Y. Unno,²³ S. Uno,^{24,21} P. Urquijo,¹¹⁹
91 Y. Ushiroda,^{24,21,127} Y. Usov,^{4,74} S. E. Vahsen,¹¹³ R. van Tonder,¹⁰⁹ G. S. Varner,¹¹³
92 K. E. Varvell,¹²⁶ A. Vinokurova,^{4,74} L. Vitale,^{104,47} V. Vorobyev,^{4,57,74} A. Vossen,¹³
93 E. Waheed,²⁴ H. M. Wakeling,⁶⁴ K. Wan,¹²⁷ W. Wan Abdullah,¹¹⁷ B. Wang,⁶²
94 C. H. Wang,⁷¹ M.-Z. Wang,⁷⁰ X. L. Wang,¹⁸ A. Warburton,⁶⁴ M. Watanabe,⁷³
95 S. Watanuki,¹⁰⁶ I. Watson,¹²⁷ J. Webb,¹¹⁹ S. Wehle,¹² M. Welsch,¹⁰⁹ C. Wessel,¹⁰⁹
96 J. Wiechczynski,⁴³ P. Wieduwilt,¹⁹ H. Windel,⁶² E. Won,⁵⁴ L. J. Wu,³⁵ X. P. Xu,⁸⁵
97 B. Yabsley,¹²⁶ S. Yamada,²⁴ W. Yan,¹²³ S. B. Yang,⁵⁴ H. Ye,¹² J. Yelton,¹¹² I. Yeo,⁵³
98 J. H. Yin,⁵⁴ M. Yonenaga,⁹⁵ Y. M. Yook,³⁵ T. Yoshinobu,⁷³ C. Z. Yuan,³⁵ G. Yuan,¹²³
99 W. Yuan,⁴¹ Y. Yusa,⁷³ L. Zani,¹ J. Z. Zhang,³⁵ Y. Zhang,¹²³ Z. Zhang,¹²³ V. Zhilich,^{4,74}
100 Q. D. Zhou,^{66,68} X. Y. Zhou,² V. I. Zhukova,⁵⁷ V. Zhulanov,^{4,74} and A. Zupanc⁸⁷

101 (Belle II Collaboration)

102 (The Belle II Collaboration)

103 ¹*Aix Marseille Université, CNRS/IN2P3, CPPM, 13288 Marseille, France*

104 ²*Beihang University, Beijing 100191, China*

105 ³*Brookhaven National Laboratory, Upton, New York 11973, U.S.A.*

106 ⁴*Budker Institute of Nuclear Physics SB RAS, Novosibirsk 630090, Russian Federation*

107 ⁵*Carnegie Mellon University, Pittsburgh, Pennsylvania 15213, U.S.A.*

108 ⁶*Centro de Investigacion y de Estudios Avanzados del*
109 *Instituto Politecnico Nacional, Mexico City 07360, Mexico*

110 ⁷*Faculty of Mathematics and Physics, Charles University, 121 16 Prague, Czech Republic*

111 ⁸*Chiang Mai University, Chiang Mai 50202, Thailand*

112 ⁹*Chiba University, Chiba 263-8522, Japan*

113 ¹⁰*Chonnam National University, Gwangju 61186, South Korea*

114 ¹¹*Consejo Nacional de Ciencia y Tecnología, Mexico City 03940, Mexico*

115 ¹²*Deutsches Elektronen-Synchrotron, 22607 Hamburg, Germany*

116 ¹³*Duke University, Durham, North Carolina 27708, U.S.A.*

117 ¹⁴*Institute of Theoretical and Applied Research*
118 *(ITAR), Duy Tan University, Hanoi 100000, Vietnam*

119 ¹⁵*Earthquake Research Institute, University of Tokyo, Tokyo 113-0032, Japan*

120 ¹⁶*Forschungszentrum Jülich, 52425 Jülich, Germany*

121 ¹⁷*Department of Physics, Fu Jen Catholic University, Taipei 24205, Taiwan*

122 ¹⁸*Key Laboratory of Nuclear Physics and Ion-beam Application (MOE) and*

- 123 *Institute of Modern Physics, Fudan University, Shanghai 200443, China*
- 124 ¹⁹*II. Physikalisches Institut, Georg-August-Universität*
- 125 *Göttingen, 37073 Göttingen, Germany*
- 126 ²⁰*Gifu University, Gifu 501-1193, Japan*
- 127 ²¹*The Graduate University for Advanced Studies (SOKENDAI), Hayama 240-0193, Japan*
- 128 ²²*Gyeongsang National University, Jinju 52828, South Korea*
- 129 ²³*Department of Physics and Institute of Natural*
- 130 *Sciences, Hanyang University, Seoul 04763, South Korea*
- 131 ²⁴*High Energy Accelerator Research Organization (KEK), Tsukuba 305-0801, Japan*
- 132 ²⁵*J-PARC Branch, KEK Theory Center, High Energy Accelerator*
- 133 *Research Organization (KEK), Tsukuba 305-0801, Japan*
- 134 ²⁶*Higher School of Economics (HSE), Moscow 101000, Russian Federation*
- 135 ²⁷*Indian Institute of Science Education and Research Mohali, SAS Nagar, 140306, India*
- 136 ²⁸*Indian Institute of Technology Bhubaneswar, Satya Nagar 751007, India*
- 137 ²⁹*Indian Institute of Technology Guwahati, Assam 781039, India*
- 138 ³⁰*Indian Institute of Technology Hyderabad, Telangana 502285, India*
- 139 ³¹*Indian Institute of Technology Madras, Chennai 600036, India*
- 140 ³²*Indiana University, Bloomington, Indiana 47408, U.S.A.*
- 141 ³³*Institute for High Energy Physics, Protvino 142281, Russian Federation*
- 142 ³⁴*Institute of High Energy Physics, Vienna 1050, Austria*
- 143 ³⁵*Institute of High Energy Physics, Chinese Academy of Sciences, Beijing 100049, China*
- 144 ³⁶*Institute of Particle Physics (Canada), Victoria, British Columbia V8W 2Y2, Canada*
- 145 ³⁷*Institute of Physics, Vietnam Academy of*
- 146 *Science and Technology (VAST), Hanoi, Vietnam*
- 147 ³⁸*Instituto de Fisica Corpuscular, Paterna 46980, Spain*
- 148 ³⁹*INFN Laboratori Nazionali di Frascati, I-00044 Frascati, Italy*
- 149 ⁴⁰*INFN Sezione di Napoli, I-80126 Napoli, Italy*
- 150 ⁴¹*INFN Sezione di Padova, I-35131 Padova, Italy*
- 151 ⁴²*INFN Sezione di Perugia, I-06123 Perugia, Italy*
- 152 ⁴³*INFN Sezione di Pisa, I-56127 Pisa, Italy*
- 153 ⁴⁴*INFN Sezione di Roma, I-00185 Roma, Italy*
- 154 ⁴⁵*INFN Sezione di Roma Tre, I-00146 Roma, Italy*
- 155 ⁴⁶*INFN Sezione di Torino, I-10125 Torino, Italy*
- 156 ⁴⁷*INFN Sezione di Trieste, I-34127 Trieste, Italy*
- 157 ⁴⁸*Advanced Science Research Center, Japan Atomic Energy Agency, Naka 319-1195, Japan*

- 158 ⁴⁹*Johannes Gutenberg-Universität Mainz, Institut*
159 *für Kernphysik, D-55099 Mainz, Germany*
- 160 ⁵⁰*Justus-Liebig-Universität Gießen, 35392 Gießen, Germany*
- 161 ⁵¹*Institut für Experimentelle Teilchenphysik, Karlsruher*
162 *Institut für Technologie, 76131 Karlsruhe, Germany*
- 163 ⁵²*Kitasato University, Sagamihara 252-0373, Japan*
- 164 ⁵³*Korea Institute of Science and Technology Information, Daejeon 34141, South Korea*
- 165 ⁵⁴*Korea University, Seoul 02841, South Korea*
- 166 ⁵⁵*Kyoto Sangyo University, Kyoto 603-8555, Japan*
- 167 ⁵⁶*Kyungpook National University, Daegu 41566, South Korea*
- 168 ⁵⁷*P.N. Lebedev Physical Institute of the Russian Academy*
169 *of Sciences, Moscow 119991, Russian Federation*
- 170 ⁵⁸*Liaoning Normal University, Dalian 116029, China*
- 171 ⁵⁹*Ludwig Maximilians University, 80539 Munich, Germany*
- 172 ⁶⁰*Luther College, Decorah, Iowa 52101, U.S.A.*
- 173 ⁶¹*Malaviya National Institute of Technology Jaipur, Jaipur 302017, India*
- 174 ⁶²*Max-Planck-Institut für Physik, 80805 München, Germany*
- 175 ⁶³*Semiconductor Laboratory of the Max Planck Society, 81739 München, Germany*
- 176 ⁶⁴*McGill University, Montréal, Québec, H3A 2T8, Canada*
- 177 ⁶⁵*Moscow Physical Engineering Institute, Moscow 115409, Russian Federation*
- 178 ⁶⁶*Graduate School of Science, Nagoya University, Nagoya 464-8602, Japan*
- 179 ⁶⁷*Kobayashi-Maskawa Institute, Nagoya University, Nagoya 464-8602, Japan*
- 180 ⁶⁸*Institute for Advanced Research, Nagoya University, Nagoya 464-8602, Japan*
- 181 ⁶⁹*Nara Women's University, Nara 630-8506, Japan*
- 182 ⁷⁰*Department of Physics, National Taiwan University, Taipei 10617, Taiwan*
- 183 ⁷¹*National United University, Miao Li 36003, Taiwan*
- 184 ⁷²*H. Niewodniczanski Institute of Nuclear Physics, Krakow 31-342, Poland*
- 185 ⁷³*Niigata University, Niigata 950-2181, Japan*
- 186 ⁷⁴*Novosibirsk State University, Novosibirsk 630090, Russian Federation*
- 187 ⁷⁵*Okinawa Institute of Science and Technology, Okinawa 904-0495, Japan*
- 188 ⁷⁶*Osaka City University, Osaka 558-8585, Japan*
- 189 ⁷⁷*Research Center for Nuclear Physics, Osaka University, Osaka 567-0047, Japan*
- 190 ⁷⁸*Pacific Northwest National Laboratory, Richland, Washington 99352, U.S.A.*
- 191 ⁷⁹*Panjab University, Chandigarh 160014, India*
- 192 ⁸⁰*Peking University, Beijing 100871, China*

- 193 ⁸¹*Punjab Agricultural University, Ludhiana 141004, India*
- 194 ⁸²*Meson Science Laboratory, Cluster for Pioneering*
195 *Research, RIKEN, Saitama 351-0198, Japan*
- 196 ⁸³*Seoul National University, Seoul 08826, South Korea*
- 197 ⁸⁴*Showa Pharmaceutical University, Tokyo 194-8543, Japan*
- 198 ⁸⁵*Soochow University, Suzhou 215006, China*
- 199 ⁸⁶*Soongsil University, Seoul 06978, South Korea*
- 200 ⁸⁷*J. Stefan Institute, 1000 Ljubljana, Slovenia*
- 201 ⁸⁸*Taras Shevchenko National Univ. of Kiev, Kiev, Ukraine*
- 202 ⁸⁹*Tata Institute of Fundamental Research, Mumbai 400005, India*
- 203 ⁹⁰*Department of Physics, Technische Universität München, 85748 Garching, Germany*
- 204 ⁹¹*Tel Aviv University, School of Physics and Astronomy, Tel Aviv, 69978, Israel*
- 205 ⁹²*Toho University, Funabashi 274-8510, Japan*
- 206 ⁹³*Department of Physics, Tohoku University, Sendai 980-8578, Japan*
- 207 ⁹⁴*Tokyo Institute of Technology, Tokyo 152-8550, Japan*
- 208 ⁹⁵*Tokyo Metropolitan University, Tokyo 192-0397, Japan*
- 209 ⁹⁶*Universidad Autonoma de Sinaloa, Sinaloa 80000, Mexico*
- 210 ⁹⁷*Dipartimento di Scienze Fisiche, Università di Napoli Federico II, I-80126 Napoli, Italy*
- 211 ⁹⁸*Dipartimento di Fisica e Astronomia, Università di Padova, I-35131 Padova, Italy*
- 212 ⁹⁹*Dipartimento di Fisica, Università di Perugia, I-06123 Perugia, Italy*
- 213 ¹⁰⁰*Dipartimento di Fisica, Università di Pisa, I-56127 Pisa, Italy*
- 214 ¹⁰¹*Università di Roma "La Sapienza," I-00185 Roma, Italy*
- 215 ¹⁰²*Dipartimento di Matematica e Fisica, Università di Roma Tre, I-00146 Roma, Italy*
- 216 ¹⁰³*Dipartimento di Fisica, Università di Torino, I-10125 Torino, Italy*
- 217 ¹⁰⁴*Dipartimento di Fisica, Università di Trieste, I-34127 Trieste, Italy*
- 218 ¹⁰⁵*Université de Montréal, Physique des Particules, Montréal, Québec, H3C 3J7, Canada*
- 219 ¹⁰⁶*Université Paris-Saclay, CNRS/IN2P3, IJCLab, 91405 Orsay, France*
- 220 ¹⁰⁷*Université de Strasbourg, CNRS, IPHC, UMR 7178, 67037 Strasbourg, France*
- 221 ¹⁰⁸*Department of Physics, University of Adelaide, Adelaide, South Australia 5005, Australia*
- 222 ¹⁰⁹*University of Bonn, 53115 Bonn, Germany*
- 223 ¹¹⁰*University of British Columbia, Vancouver, British Columbia, V6T 1Z1, Canada*
- 224 ¹¹¹*University of Cincinnati, Cincinnati, Ohio 45221, U.S.A.*
- 225 ¹¹²*University of Florida, Gainesville, Florida 32611, U.S.A.*
- 226 ¹¹³*University of Hawaii, Honolulu, Hawaii 96822, U.S.A.*

- 227 ¹¹⁴*University of Heidelberg, 68131 Mannheim, Germany*
- 228 ¹¹⁵*Faculty of Mathematics and Physics, University of Ljubljana, 1000 Ljubljana, Slovenia*
- 229 ¹¹⁶*University of Louisville, Louisville, Kentucky 40292, U.S.A.*
- 230 ¹¹⁷*National Centre for Particle Physics, University Malaya, 50603 Kuala Lumpur, Malaysia*
- 231 ¹¹⁸*University of Maribor, 2000 Maribor, Slovenia*
- 232 ¹¹⁹*School of Physics, University of Melbourne, Victoria 3010, Australia*
- 233 ¹²⁰*University of Mississippi, University, Mississippi 38677, U.S.A.*
- 234 ¹²¹*University of Miyazaki, Miyazaki 889-2192, Japan*
- 235 ¹²²*University of Pittsburgh, Pittsburgh, Pennsylvania 15260, U.S.A.*
- 236 ¹²³*University of Science and Technology of China, Hefei 230026, China*
- 237 ¹²⁴*University of South Alabama, Mobile, Alabama 36688, U.S.A.*
- 238 ¹²⁵*University of South Carolina, Columbia, South Carolina 29208, U.S.A.*
- 239 ¹²⁶*School of Physics, University of Sydney, New South Wales 2006, Australia*
- 240 ¹²⁷*Department of Physics, University of Tokyo, Tokyo 113-0033, Japan*
- 241 ¹²⁸*Kavli Institute for the Physics and Mathematics of the*
- 242 *Universe (WPI), University of Tokyo, Kashiwa 277-8583, Japan*
- 243 ¹²⁹*University of Victoria, Victoria, British Columbia, V8W 3P6, Canada*
- 244 ¹³⁰*Virginia Polytechnic Institute and State University, Blacksburg, Virginia 24061, U.S.A.*
- 245 ¹³¹*Wayne State University, Detroit, Michigan 48202, U.S.A.*
- 246 ¹³²*Yamagata University, Yamagata 990-8560, Japan*
- 247 ¹³³*Alikhanyan National Science Laboratory, Yerevan 0036, Armenia*
- 248 ¹³⁴*Yonsei University, Seoul 03722, South Korea*

Abstract

250 Tag-side reconstruction is an important method for reconstructing B meson decays with missing
 251 energy. The Belle II tag-side reconstruction algorithm, Full Event Interpretation, relies on a hier-
 252 archical reconstruction of B meson decays with multivariate classification employed at each stage
 253 of reconstruction. Given the large numbers of classifiers employed and decay chains reconstructed,
 254 the performance of the algorithm on data and simulation differs significantly. Here, calibration
 255 factors are derived to correct for this effect for the case of hadronic tag-sides using $B \rightarrow X\ell\nu$
 256 decays in 34.6 fb^{-1} of Belle II data. For a loose selection on the tag-side B multivariate classifier
 257 the calibration factors are 0.65 ± 0.02 and 0.83 ± 0.03 for tag-side B^+ and B^0 mesons, respectively.

258 1. INTRODUCTION

259 The Belle II experiment [1] is an e^+e^- collider experiment in Japan, which began its
260 main physics runs in early 2019 and has so far collected 74 fb^{-1} of data at a centre-of-mass
261 (CM) energy, \sqrt{s} , corresponding to the mass of the $\Upsilon(4S)$ resonance. The clean environment
262 of e^+e^- collisions together with the unique event topology of Belle II, in which an $\Upsilon(4S)$
263 meson is produced and subsequently decays into a pair of B mesons, allows a wide range of
264 physics measurements to be performed which are difficult or impossible at hadron colliders.
265 In particular, measurements in which there is missing energy, which includes semileptonic
266 decays with missing neutrinos, can benefit substantially from the additional constraints
267 provided by the collision environment of Belle II. This includes the measurement of the ratio
268 of branching fractions, $R(D^*) = \mathcal{B}(B \rightarrow D^{(*)}\tau\nu)/\mathcal{B}(B \rightarrow D^{(*)}\ell\nu)$, inclusive determinations
269 of the CKM matrix elements $|V_{ub}|$ and $|V_{cb}|$ from $X_{u/c}\ell\nu$ decays and searches for the rare
270 decay $b \rightarrow s\nu\bar{\nu}$.

271 Full Event Interpretation [2] is an algorithm for tag-side B meson reconstruction at Belle
272 II. The algorithm utilises a hierarchical reconstruction of exclusive decay chains of B mesons,
273 with multivariate classifiers utilised to identify each unique sub-decay channel. Given the
274 large number of decay chains reconstructed and multivariate classifiers employed there can
275 be significant differences between the tag-side reconstruction efficiency in simulation and
276 data. In order to correct for this, a calibration can be performed by measuring a decay
277 with a well known branching fraction and sufficient available statistics after selection. A
278 suitable choice given the current Belle II dataset is inclusive $B \rightarrow X\ell\nu$ decays because
279 of the substantial branching fraction of $\sim 20\%$. This is also an ideal choice of decay to
280 demonstrate the applicability of tag-side reconstruction to inclusive semileptonic decays in
281 Belle II data.

282 2. DETECTOR AND SIMULATION

283 The Belle II detector [1, 3] operates at the SuperKEKB asymmetric-energy electron-
284 positron collider [4], located at the KEK laboratory in Tsukuba, Japan. The detector
285 consists of several nested detector subsystems arranged around the beam pipe in a cylindrical
286 geometry.

287 The innermost subsystem is the vertex detector, which includes two layers of silicon pixel
288 detectors and four outer layers of silicon strip detectors. Currently, the second pixel layer is
289 installed in only a small part of the solid angle, while the remaining vertex detector layers
290 are fully installed. Most of the tracking volume consists of a helium- and ethane-based
291 small-cell drift chamber.

292 Outside the drift chamber, a Cherenkov-light imaging and time-of-propagation detec-
293 tor provides charged-particle identification in the barrel region. In the forward endcap,
294 this function is provided by a proximity-focusing, ring-imaging Cherenkov detector with an
295 aerogel radiator. Further out is an electromagnetic calorimeter, consisting of a barrel and
296 two endcap sections made of CsI(Tl) crystals. A uniform 1.5 T magnetic field is provided
297 by a superconducting solenoid situated outside the calorimeter. Multiple layers of scintil-
298 lators and resistive plate chambers, located between the magnetic flux-return iron plates,

299 constitute the K_L and muon identification system.

300 The data used in this analysis were collected at a CM energy, \sqrt{s} , of 10.58 GeV, cor-
 301 responding to the mass of the $\Upsilon(4S)$ resonance. The energies of the electron and positron
 302 beams are 7 GeV and 4 GeV, respectively, resulting in a boost of $\beta\gamma = 0.28$ of the CM frame
 303 relative to the lab frame. The integrated luminosity of the data is 34.6 fb^{-1} . In addition, a
 304 smaller sample of 3.23 fb^{-1} off-resonance data was collected at a CM energy of 10.52 GeV

305 The analysis utilises several samples of simulated events. These include a sample of
 306 $e^+e^- \rightarrow B\bar{B}$ with generic B -meson decays, generated with EvtGen, and corresponding to an
 307 integrated luminosity of 100 fb^{-1} . A 100 fb^{-1} sample of continuum $e^+e^- \rightarrow q\bar{q}$ ($q = u, d, s, c$)
 308 is simulated with KKMC [5] interfaced with PYTHIA [6]. All data samples were analyzed
 309 (and, for MC events, generated and simulated) in the basf2 [7] framework.

310 3. THE ALGORITHM

311 The FEI employs a hierarchical reconstruction of exclusive B meson decay chains, in
 312 which each unique decay channel of a particle has its own designated multivariate classifier.
 313 The algorithm utilises several stages of reconstruction, which are shown in Figure 1. The
 314 algorithm starts by selecting candidates for stable particles, which include muons, electrons,
 315 pions, kaons and photons, from tracks and EM clusters in the event. Subsequently, the
 316 algorithm carries out several stages of reconstruction of intermediate particles such as π^0 ,
 317 K_S^0 , J/ψ , D and D^* mesons and, in addition, Σ , Λ and Λ_c baryons. The addition of baryonic
 318 modes was a recent extension of the algorithm. Intermediate particles are reconstructed in
 319 specific decay modes from a combination of stable and other intermediate particle candi-
 320 dates. The final stage of the algorithm reconstructs the B^+ and B^0 mesons in 36 (8) and 31
 321 (8) hadronic (semileptonic) modes.

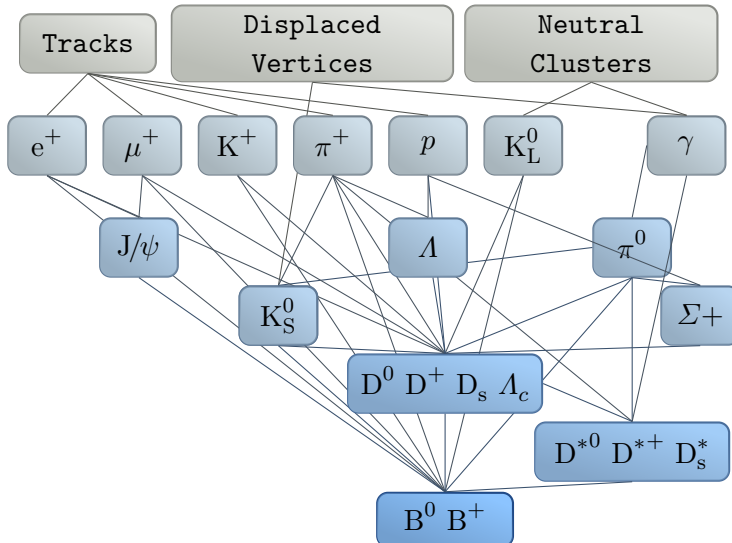


FIG. 1. The stages of reconstruction employed by Full Event Interpretation.

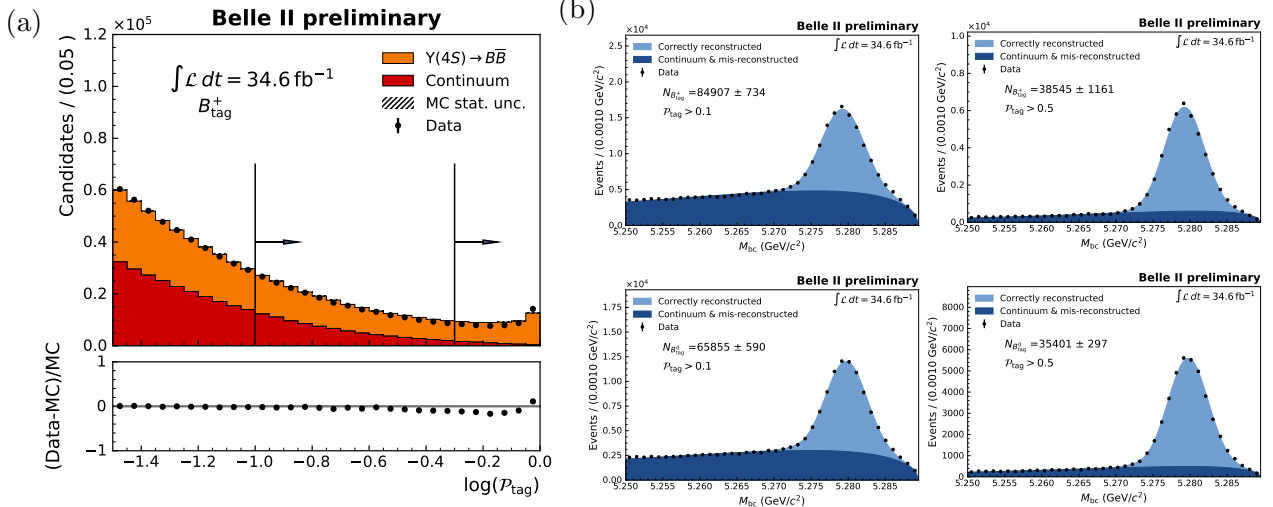


FIG. 2. (a) Comparison of the distribution of $\log \mathcal{P}_{\text{tag}}$ in early Belle II data to the shape expectation from simulation. Here $\log \mathcal{P}_{\text{tag}}$ is the logarithm of the tag-side B^+ meson classifier output, \mathcal{P}_{tag} . Reference selection criteria of $\mathcal{P}_{\text{tag}} > 0.1$ and $\mathcal{P}_{\text{tag}} > 0.5$ are illustrated. (b) Fits to the beam-constrained-mass, M_{bc} , distribution of reconstructed B^+ (top) and B^0 (bottom) tag-side B mesons in data. A looser selection criteria of $\mathcal{P}_{\text{tag}} > 0.1$ (left) and a tighter selection criteria of $\mathcal{P}_{\text{tag}} > 0.5$ are applied on the B meson classifier \mathcal{P}_{tag} to select samples with different levels of purity.

322 Each stage consists of pre-reconstruction and post-reconstruction steps. In the pre-
 323 reconstruction step, candidates for particles are reconstructed, an initial pre-selection is ap-
 324 plied and a best candidate selection is made on a discriminating variable. Subsequently, in
 325 the post-reconstruction step, vertex fits are performed where applicable, pre-trained classi-
 326 fiers are applied and a best-candidate selection is made on the classifier output. Classifiers
 327 for stable particles utilise kinematic and particle identification information as features, mean-
 328 while, intermediate and B classifiers utilise the kinematic information from all daughters,
 329 daughter classifier outputs and information from vertex fits as features.

330 The algorithm requires a training procedure, in which all of the particle classifiers are
 331 trained. For the calibration studies performed here the training was performed on simulated
 332 $\Upsilon(4S) \rightarrow B\bar{B}$ events corresponding to an integrated luminosity of 100fb^{-1} . The training of
 333 the algorithm utilises an equivalent reconstruction procedure to produce training datasets
 334 for each particle decay channel classifier.

335 Subsequently, the tag-side B classifier, \mathcal{P}_{tag} , can be used to select a pure sample of cor-
 336 rectly reconstructed tag-side B mesons. This is demonstrated in Figure 3, which shows
 337 fits to the beam constrained mass distribution, $M_{\text{bc}} = \sqrt{E_{\text{beam}}^2 - (p_{\text{tag}}^{\text{CM}})^2}$, for reconstructed
 338 tag-side B^0 and B^+ mesons, for selections requiring \mathcal{P}_{tag} to be greater than 0.1 and 0.5. The
 339 contribution from correctly reconstructed tag-side B mesons is parametrised by a Crystal
 340 Ball [8], meanwhile, background from $e^+e^- \rightarrow q\bar{q}$ ($q = u, d, s, c$) and incorrectly recon-
 341 structed B mesons are modelled with an Argus function [9]. By applying a tighter selection
 342 on the classifier output a higher purity sample of tag-side B mesons can be selected
 343 with the sacrifice of a lower tag-side efficiency, which is proportional to the yield of correctly
 344 reconstructed tag-side B mesons.

345 **4. SELECTION**

346 The selection process begins by requiring that there is at most one tag-side in each event.
 347 This is achieved by selecting the tag-side candidate with the highest tag-side B classifier
 348 output, \mathcal{P}_{tag} . For correctly reconstructed tags the beam energy difference, ΔE , should peak
 349 around 0 with some mode dependent resolution, which is assymmetric with a skew towards
 350 lower values given modes containing $\pi^0 \rightarrow \gamma\gamma$ decays. Therefore, an asymmetric requirement
 351 is placed on the beam energy difference to lie in the range $-0.15 < \Delta E < 0.1$ GeV. In order
 352 to reduce background from $e^+e^- \rightarrow q\bar{q}$ events a requirement on an event level normalised 2nd
 353 Fox Wolfram moment to be less than 0.3 is made. Figure 3 shows a breakdown of the m_{bc}
 354 distribution in data into several categories of tag-side decay mode after the above selection
 355 and a requirement that $\mathcal{P}_{\text{tag}} > 0.01$. It can be seen that the dominant tag-side decay mode
 356 categories are $D\pi$, $D^*\pi$, $Dn\pi$ and $D^*n\pi$. The recently added baryonic modes result in a
 357 small increase in the tag-side efficiency boosting the number of correctly reconstructed tag-
 358 sides by roughly 3% (2%) for B^+ (B^0) tag-sides. The final selection applied to the tag-side
 359 is a requirement that m_{bc} is greater than 5.27 GeV/c^2 , which selects the region containing
 360 correctly reconstructed tag-sides as can be seen in Figure 3.

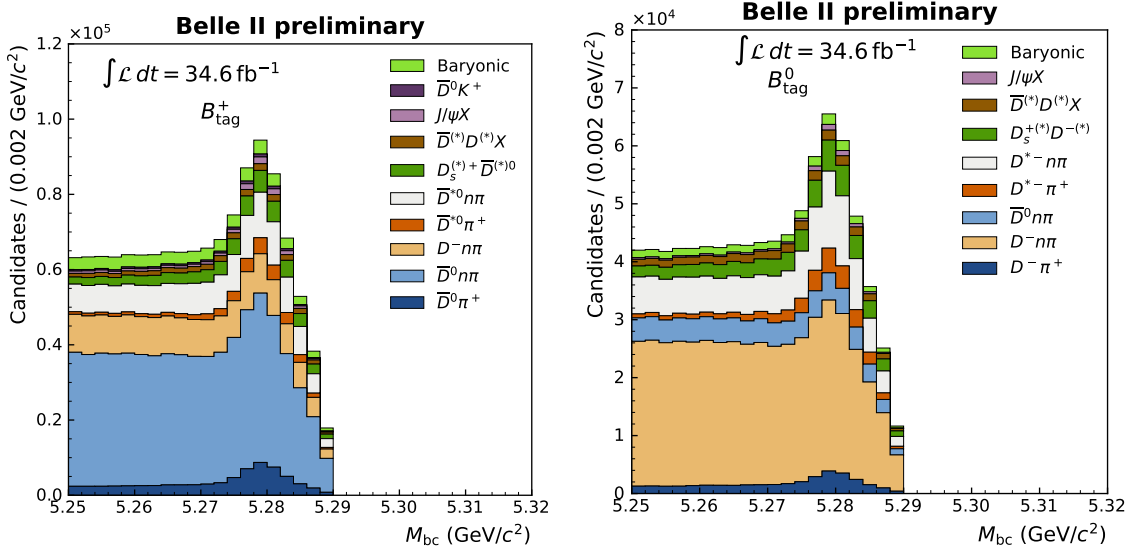


FIG. 3. Contribution of different tag-side decay modes to the M_{bc} distribution in data for B^+ (left) and B^0 (right) tag-sides when $\mathcal{P}_{\text{tag}} > 0.01$. Contributions from the newly added baryonic modes can also be seen.

361 After the tag-side selection the signal side selection is applied. In particular, a lepton
 362 is selected with $p_\ell^* > 1$ GeV/c , where p_ℓ^* refers to the momentum of the lepton in the B
 363 rest frame, which can be determined using the 4-momentum of the recoiling tag-side. The
 364 distance of closest approach between each track and the interaction point is required to
 365 be less than 2 cm along the z direction (parallel to the beams) and less than 0.5 cm in the
 366 transverse $r - \phi$ plane. Particle identification information from several sub-detectors, includ-
 367 ing Cherenkov time of propagation (TOP), Aerogel ring imaging Cherenkov and dedicated
 368 muon detectors, is combined into a likelihood for each of electron and muon hypotheses in

369 order to select each lepton species. The selection on p_ℓ^* to be greater than 1 GeV/c was
 370 motivated by the fact that lepton identification performance is found to degrade significantly
 371 below 1 GeV/c.

372 5. CALIBRATION PROCEDURE

373 The calibration factor is defined as $\epsilon = N_{X\ell\nu}^{\text{Data}}/N_{X\ell\nu}^{\text{MC}}$, where the yield of $X\ell\nu$ decays in
 374 data, $N_{X\ell\nu}^{\text{Data}}$, is determined by fitting the p_ℓ^* distribution. Meanwhile, $N_{X\ell\nu}^{\text{MC}}$ is the expected
 375 yield as determined using Monte Carlo simulation.

376 The fitting procedure relies on maximising a binned likelihood, \mathcal{L} , defined by the following
 377 equation,

$$-2 \log \mathcal{L} = -2 \log \prod_i \text{Poisson}(\nu_i^{\text{obs}}, \nu_i^{\text{exp}}) + \theta^T \Sigma_\theta^{-1} \theta + (k - k_{\text{constraint}})^T \Sigma_{\text{constraints}}^{-1} (k - k_{\text{constraint}}) \quad (1)$$

378 where ν_i^{obs} is the number of events observed in a given bin i . The number of expected events
 379 is given by:

$$\nu_i^{\text{exp}}(\nu^j, \theta_i^j) = \sum_j \nu^j \frac{p_i^j (1 + \theta_i^j)}{\sum_k p_k^j (1 + \theta_k^j)}, \quad (2)$$

380 where p_i^j defines the probability for a decay of type j to end up in bin i . The nuisance
 381 parameters, θ_i^j , account for both MC template statistics and additional systematic effects.
 382 The associated bin to bin correlations between systematic uncertainties are accounted for in
 383 the covariance matrix, Σ_θ .

384 The fit has three yields associated with three pdfs describing the $X\ell\nu$ signal decays,
 385 background from $e^+e^- \rightarrow q\bar{q}$ events and finally background in which the lepton is fake or
 386 secondary. Secondary here refers to the situation in which the lepton is not directly produced
 387 in the decay of B meson but rather through a secondary cascade decay of a charmed meson.
 388 The $X\ell\nu$ signal pdf is further broken down into four sub-components, which include $D^*\ell\nu$,
 389 $D\ell\nu$, $X_u\ell\nu$ and any remaining $X_c\ell\nu$ decays ($D^{**}\ell\nu$ and $D^{(*)}n\pi\ell\nu$). The relative contributions
 390 of these four components are parametrised by three fractions (f_D , f_{D^*} and f_{X_u}).

391 The last term, $(k - k_{\text{constraint}})^T \Sigma_{\text{constraints}}^{-1} (k - k_{\text{constraint}})$, in Equation 1 allows for con-
 392 straints on parameters in the fit. The parameter vector $k = (N(e^+e^- \rightarrow q\bar{q}), f_D, f_{D^*}, f_{X_u})$
 393 contains the subset of fit parameters, which are subject to constraints. The vector $k_{\text{constraints}}$
 394 contains the corresponding nominal values that these parameters are constrained to. The
 395 continuum yield, $N(e^+e^- \rightarrow q\bar{q})$, is constrained to its expectation based on counting off-
 396 resonance events and scaling up to account for luminosity. The constraints on the three
 397 fractions are obtained from MC expectation after all branching fraction corrections are
 398 made.

399 Fit results for the channels B^+e^- , $B^+\mu^-$, B^0e^- and $B^0\mu^-$ with a selection of $\mathcal{P} > 0.001$
 400 are shown in Figure 4. A good agreement between data and the fitted models is observed
 401 across all channels. Figure 5 shows the $B^+\ell^-$ fit channels in the region where $p_\ell^* > 2$ GeV/c.

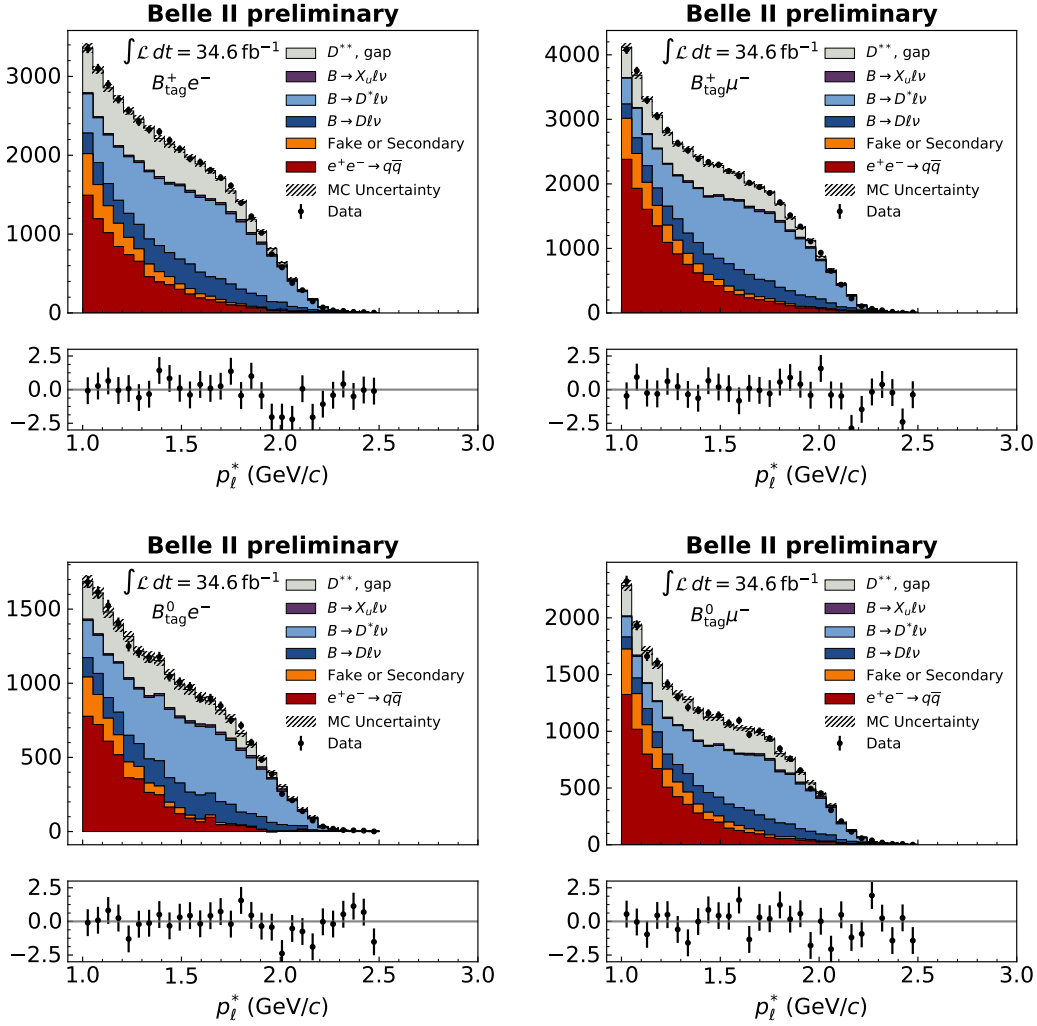


FIG. 4. fits to p_ℓ^* in data for charged or neutral tag-sides combined with electrons. The $X\ell\nu$ template is either plotted separated into its component pdfs (left) or as a whole (right).

402 In this region the contribution from $B \rightarrow X_u \ell \nu$ decays becomes evident due to the lower
 403 kinematic endpoint of $B \rightarrow X_c \ell \nu$ decays. This allows one to better constrain the albeit
 404 small contribution from $X_u \ell \nu$ decays.

405 6. SOURCES OF SYSTEMATIC UNCERTAINTY

406 The calibration procedure is affected by a number of sources of systematic uncertainty.
 407 These can both influence the determination of the MC expected yield, $N_{X\ell\nu}^{\text{MC}}$ (normalisation
 408 uncertainties) or the shapes of pdfs entering the fitting procedure (shape uncertainties).

409 We first discuss the estimation of systematic uncertainties for the MC expected yield,
 410 $N_{X\ell\nu}^{\text{MC}}$. The first source of systematic uncertainty considered is that arising from the knowl-

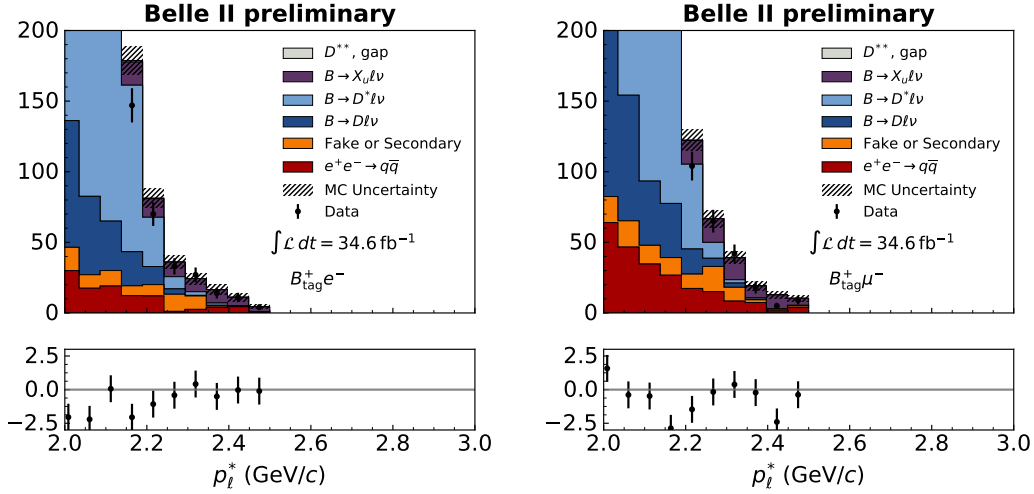


FIG. 5. fits to p_ℓ^* in data in the region $p_\ell^* > 2$ GeV/c. This region is enhanced in $B \rightarrow X_u \ell \nu$ decays relative to $B \rightarrow X_c \ell \nu$ decays due to the lower kinematic endpoint for $B \rightarrow X_c \ell \nu$ decays.

411 edge of the $X\ell\nu$ branching fractions. Several branching fractions of $X\ell\nu$ decay modes includ-
 412 ing $D\ell\nu$, $D^*\ell\nu$ and $X_u\ell\nu$ were first corrected to their latest PDG values. After having applied
 413 these corrections the overall charged and neutral $B \rightarrow X\ell\nu$ branching fractions were scaled
 414 to match those in the PDG: $\mathcal{B}(B^+ \rightarrow X\ell\nu) = 10.99 \pm 0.28$ and $\mathcal{B}(B^0 \rightarrow X\ell\nu) = 10.33 \pm 0.28$.
 415 The corresponding uncertainties are treated as a source of systematic uncertainty. In addi-
 416 tion to correcting several branching fractions, the form factors of $D\ell\nu$ and $D^*\ell\nu$ decays
 417 are updated to the BGL parametrisations of references [10, 11], with the central parameter
 418 values in reference [12]. The associated uncertainties on the form factor parameters of these
 419 parameterisations are propagated in the analysis using up and down one sigma variations in
 420 an uncorrelated eigenbasis of form factor parameters of the corresponding BGL parametri-
 421 sations. The form factor uncertainties can influence $N_{X\ell\nu}^{\text{MC}}$ due to the selection of $p_\ell^* > 1$
 422 GeV/c.

423 The next sources of uncertainty considered relate to tracking and particle identification.
 424 Due to mismatches in the reconstruction of tracks between simulation and data, a system-
 425 atic error of 0.91% is assigned for the single signal-side track. The performance of lepton
 426 identification also differs between data and MC. Consequently, the lepton identification
 427 rates and $\pi \rightarrow \ell$ fake rates are corrected in bins of lepton p and θ using corrections derived
 428 from samples of $J/\psi \rightarrow \ell^+ \ell^-$ and $K_S^0 \rightarrow \pi^+ \pi^-$ decays in data. The systematic uncertainty
 429 associated with these corrections is determined by generating gaussian variations on these
 430 weights according to their systematic and statistical uncertainties, while assuming that the
 431 systematic uncertainties across bins are 100% correlated. The final considered source of
 432 systematic uncertainty on $N_{X\ell\nu}^{\text{MC}}$ is the statistical size of the MC sample used to estimate
 433 $N_{X\ell\nu}^{\text{MC}}$.

434 A number of systematic effects can impact the expected p_ℓ^* distribution from simulation.
 435 These include the Monte Carlo statistics, the $D^{(*)}\ell\nu$ form factors, lepton identification and
 436 the composition of $X\ell\nu$ decays. The uncertainty associated with the composition of $X\ell\nu$
 437 is propagated into the fit through the freedom of the $X\ell\nu$ pdf to change according to

438 aforementioned sub-pdf fractions. A multivariate Gaussian constraint on these fractions is
 439 estimated, which accounts for the PDG uncertainty on several branching fraction updates
 440 and Monte Carlo statistics. Given that the contribution from $D^{**}\ell\nu$ and $D^{(*)}n\pi\ell\nu$ is not very
 441 well known, the overall branching fraction of these transitions is assigned a 20% uncertainty.

442 The shape impact for the remaining systematic sources of uncertainty are accounted
 443 for by using the nuisance parameters associated with each bin of a sub-pdf. For each
 444 systematic source of uncertainty, s , a $N_{\text{dim}} \times N_{\text{dim}}$ covariance matrix, Σ_s , is estimated,
 445 where $N_{\text{dim}} = N_{\text{bins}} \times N_{\text{pdfs}}$. For lepton identification, Σ_{LID} , is estimated by filling histograms
 446 with each independent weight variation. Meanwhile, for the $D^{(*)}$ form factors, $\Sigma_{D^{(*)}\text{FF}}$ is
 447 estimated by combining covariance matrices associated with up and down one sigma eigen-
 448 variations of BGL form factor parameters. Lastly for MC statistics, Σ_{MC} is determined
 449 using poisson statistics and is purely diagonal. The total covariance matrix $\Sigma_{\theta} = \sum_s \Sigma_s$ is
 450 used in the nuisance parameter constraint term of Equation 1.

451 7. RESULTS

452 Final results for the calibration factors as determined from the fitted yields are shown in
 453 Figure 6. The corresponding numerical results can be found in Appendix A along with the
 454 simulated and fitted yields of $X\ell\nu$ decays. Calibration factors for B^0 and B^+ tag-sides are
 455 found to agree well across lepton channel with the B^+ and B^0 calibration factors ranging
 456 from 0.60-0.63 and 0.70-0.83, respectively. For B^0 tag-sides the calibration factors with a
 457 looser selection on the tag-side B classifier output, $\mathcal{P}_{B_{\text{tag}}^0}$, are generally observed to be higher.
 458 This appears to be due to the fact that a looser cut increases the contribution of certain
 459 modes in the lower purity region. The final breakdown of sources uncertainties for the
 460 calibration factors are shown Table II for the selection choice of $\mathcal{P} > 0.001$. The dominant
 461 systematic uncertainty is associated with the shape freedom in the fit, which ranges from
 462 2-4% depending on the channel. The next largest sources of uncertainty are those associated
 463 with $\mathcal{B}(B^{+0} \rightarrow X\ell\nu)$ (2.1%) and tracking (0.91%).

464 The calibration factors are subsequently averaged across lepton modes as displayed in
 465 Table I and in Figure 6. The averaging procedure uses a weighted average, which accounts
 466 for the relative uncertainties and correlations of the measurements. In particular, the un-
 467 certainties from tracking, $\mathcal{B}(B^{+0} \rightarrow X\ell\nu)$, and the $D^{(*)}\ell\nu$ form factors are deemed 100%
 468 correlated.

469 The final calibration factors, ϵ_{cal} , in Table I can be applied in order to correct the tag-side
 470 efficiency in simulation, $\epsilon_{\text{tag}}^{\text{MC}}$. In Figure 6 the corrected tag-side efficiency from simulation,
 471 $\epsilon_{\text{tag}}^{\text{MC}} \times \epsilon_{\text{cal}}$, is shown against purity, for the selections $\mathcal{P}_{\text{tag}} > 0.001, 0.01$ and 0.1 . Here
 472 the tag-side efficiency, $\epsilon_{\text{tag}}^{\text{MC}}$, refers to ratio of the number of events containing a correctly
 473 reconstructed tag-side in the region $m_{bc} > 5.27$ to the total number of simulated $\Upsilon(4S) \rightarrow$
 474 $B\bar{B}$ events. Meanwhile the purity is the ratio of the number of events containing a correctly
 475 reconstructed tag-sides in this region to the number of events constraining a reconstructed
 476 tag-side.

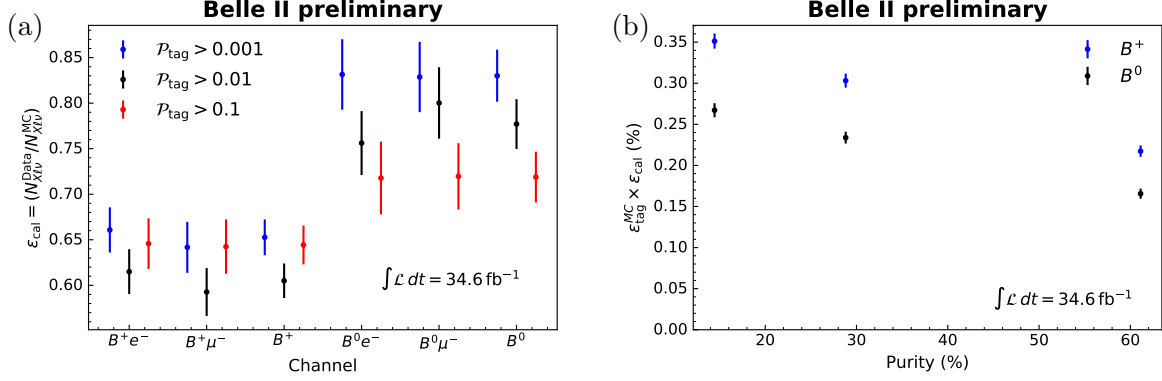


FIG. 6. (a) Calibration factors for each of the different channels and different signal probability, \mathcal{P}_{tag} , selection choices. A good agreement is seen between muon and electron channels. (b) $\epsilon_{\text{tag}}^{\text{MC}} \times \epsilon_{\text{cal}}$ against purity for $\mathcal{P}_{\text{tag}} > 0.001, 0.01$ and 0.1 for B^0 and B^+ mesons.

B^+		
$\mathcal{P}_{\text{tag}} >$	ϵ	uncertainty [%]
0.001	0.65 ± 0.02	3.0
0.01	0.61 ± 0.02	3.1
0.1	0.64 ± 0.02	3.3
B^0		
$\mathcal{P}_{\text{tag}} >$	ϵ	uncertainty [%]
0.001	0.83 ± 0.03	3.4
0.01	0.78 ± 0.03	3.5
0.1	0.72 ± 0.03	3.9

TABLE I. Final calibration factors averaged over lepton type. A weighted average taking into account the uncertainties and correlated systematics was used.

Channel	MC Stat.	$\mathcal{B}(B^{0/+} \rightarrow Xl\nu)$	Tracking	$Dl\nu$	FF	Lepton ID	$D^*l\nu$	FF	Fit Stat.	Fit Model
B^+e^-	0.39	2.09	0.91	0.06	0.76	0.41	0.93	2.67		
$B^+\mu^-$	0.37	2.1	0.91	0.06	2.13	0.38	0.86	2.93		
B^0e^-	0.62	2.1	0.91	0.07	0.73	0.43	1.22	3.72		
$B^0\mu^-$	0.6	2.09	0.91	0.06	2.13	0.41	1.19	3.17		

TABLE II. A break down of the percentage contribution from different sources of uncertainty on the calibration factors for the selection $\mathcal{P}_{\text{tag}} > 0.001$.

477 8. CONCLUSIONS

478 At Belle II hadronic tag-side reconstruction will be a critical part of the physics program
479 allowing a number of challenging final states with missing energy to be measured. This
480 includes measurements of $R(D^{(*)})$ with $B \rightarrow D^{(*)}\tau\nu$ decays, measurements of the CKM

481 matrix elements V_{ub} and V_{cb} using inclusive $B \rightarrow X_{c/u}\ell\nu$ transitions and searches for the
482 rare decay $b \rightarrow s\nu\bar{\nu}$

483 The Belle II experiment’s tag-side reconstruction algorithm, Full event interpretation,
484 relies on a hierarchical reconstruction of around 10000 B meson decays with over 200 mul-
485 tivariate classifiers. In order to employ the algorithm in a physics analysis it is necessary
486 to account for differences in the performance of the algorithm between data and simulation.
487 Here, first calibration factors were derived in order to correct for these effects by measuring
488 a well-known signal side of $B \rightarrow X\ell\nu$ decays. Calibration factors are determined for both
489 B^0 and B^+ mesons for a range of selections on the tag-side B multivariate classifier. For a
490 loose selection, the calibration factors are 0.653 ± 0.020 and 0.830 ± 0.029 for tag-side B^+
491 and B^0 mesons, respectively.

492 9. ACKNOWLEDGEMENTS

493 We thank the SuperKEKB group for the excellent operation of the accelerator; the KEK
494 cryogenics group for the efficient operation of the solenoid; and the KEK computer group
495 for on-site computing support. This work was supported by the following funding sources:
496 Science Committee of the Republic of Armenia Grant No. 18T-1C180; Australian Research
497 Council and research grant Nos. DP180102629, DP170102389, DP170102204, DP150103061,
498 FT130100303, and FT130100018; Austrian Federal Ministry of Education, Science and Re-
499 search, and Austrian Science Fund No. P 31361-N36; Natural Sciences and Engineering
500 Research Council of Canada, Compute Canada and CANARIE; Chinese Academy of Sci-
501 ences and research grant No. QYZDJ-SSW-SLH011, National Natural Science Foundation
502 of China and research grant Nos. 11521505, 11575017, 11675166, 11761141009, 11705209,
503 and 11975076, LiaoNing Revitalization Talents Program under contract No. XLYC1807135,
504 Shanghai Municipal Science and Technology Committee under contract No. 19ZR1403000,
505 Shanghai Pujiang Program under Grant No. 18PJ1401000, and the CAS Center for Excel-
506 lence in Particle Physics (CCEPP); the Ministry of Education, Youth and Sports of the Czech
507 Republic under Contract No. LTT17020 and Charles University grants SVV 260448 and
508 GAUK 404316; European Research Council, 7th Framework PIEF-GA-2013-622527, Hori-
509 zon 2020 Marie Skłodowska-Curie grant agreement No. 700525 ‘NIOBE,’ and Horizon 2020
510 Marie Skłodowska-Curie RISE project JENNIFER2 grant agreement No. 822070 (European
511 grants); L’Institut National de Physique Nucléaire et de Physique des Particules (IN2P3) du
512 CNRS (France); BMBF, DFG, HGF, MPG, AvH Foundation, and Deutsche Forschungsge-
513 meinschaft (DFG) under Germany’s Excellence Strategy – EXC2121 “Quantum Universe”
514 – 390833306 (Germany); Department of Atomic Energy and Department of Science and
515 Technology (India); Israel Science Foundation grant No. 2476/17 and United States-Israel
516 Binational Science Foundation grant No. 2016113; Istituto Nazionale di Fisica Nucleare
517 and the research grants BELLE2; Japan Society for the Promotion of Science, Grant-in-Aid
518 for Scientific Research grant Nos. 16H03968, 16H03993, 16H06492, 16K05323, 17H01133,
519 17H05405, 18K03621, 18H03710, 18H05226, 19H00682, 26220706, and 26400255, the Na-
520 tional Institute of Informatics, and Science Information NETwork 5 (SINET5), and the Min-
521 istry of Education, Culture, Sports, Science, and Technology (MEXT) of Japan; National
522 Research Foundation (NRF) of Korea Grant Nos. 2016R1D1A1B01010135, 2016R1D1A1B-
523 02012900, 2018R1A2B3003643, 2018R1A6A1A06024970, 2018R1D1A1B07047294, 2019K1-

524 A3A7A09033840, and 2019R1I1A3A01058933, Radiation Science Research Institute, For-
525 eign Large-size Research Facility Application Supporting project, the Global Science Ex-
526 perimental Data Hub Center of the Korea Institute of Science and Technology Informa-
527 tion and KREONET/GLORIAD; Universiti Malaya RU grant, Akademi Sains Malaysia
528 and Ministry of Education Malaysia; Frontiers of Science Program contracts FOINS-296,
529 CB-221329, CB-236394, CB-254409, and CB-180023, and SEP-CINVESTAV research grant
530 237 (Mexico); the Polish Ministry of Science and Higher Education and the National Sci-
531 ence Center; the Ministry of Science and Higher Education of the Russian Federation,
532 Agreement 14.W03.31.0026; University of Tabuk research grants S-1440-0321, S-0256-1438,
533 and S-0280-1439 (Saudi Arabia); Slovenian Research Agency and research grant Nos. J1-
534 9124 and P1-0135; Agencia Estatal de Investigacion, Spain grant Nos. FPA2014-55613-
535 P and FPA2017-84445-P, and CIDEAGENT/2018/020 of Generalitat Valenciana; Ministry
536 of Science and Technology and research grant Nos. MOST106-2112-M-002-005-MY3 and
537 MOST107-2119-M-002-035-MY3, and the Ministry of Education (Taiwan); Thailand Cen-
538 ter of Excellence in Physics; TUBITAK ULAKBIM (Turkey); Ministry of Education and
539 Science of Ukraine; the US National Science Foundation and research grant Nos. PHY-
540 1807007 and PHY-1913789, and the US Department of Energy and research grant Nos. DE-
541 AC06-76RLO1830, DE-SC0007983, DE-SC0009824, DE-SC0009973, DE-SC0010073, DE-
542 SC0010118, DE-SC0010504, DE-SC0011784, DE-SC0012704; and the National Foundation
543 for Science and Technology Development (NAFOSTED) of Vietnam under contract No
544 103.99-2018.45.

-
- 545 [1] E. Kou et al., *The Belle II Physics Book*, PTEP **2019** (2019) no. 12, 123C01.
546 [2] T. Keck et al., *The Full Event Interpretation – An exclusive tagging algorithm for the Belle*
547 *II experiment*, Comput Softw Big Sci **3** (2019) 6.
548 [3] T. Abe et al., Belle II Collaboration, *Belle II Technical Design Report*, arXiv:1011.0352
549 [physics.ins-det].
550 [4] K. Akai, K. Furukawa, and H. Koiso, SuperKEKB Collaboration, *SuperKEKB Collider*,
551 Nucl. Instrum. Meth. **A907** (2018) 188–199.
552 [5] B. Ward, S. Jadach, and Z. Was, *Precision calculation for $e^+ e^- \rightarrow \gamma 2f$: The KK MC*
553 *project*, Nucl. Phys. B Proc. Suppl. **116** (2003) 73–77, arXiv:hep-ph/0211132.
554 [6] T. Sjostrand, S. Mrenna, and P. Z. Skands, *A Brief Introduction to PYTHIA 8.1*, Comput.
555 Phys. Commun. **178** (2008) 852–867, arXiv:0710.3820 [hep-ph].
556 [7] T. Kuhr, C. Pulvermacher, M. Ritter, T. Hauth, and N. Braun, Belle-II Framework Software
557 Group, *The Belle II Core Software*, Comput. Softw. Big Sci. **3** (2019) no. 1, 1,
558 arXiv:1809.04299 [physics.comp-ph].
559 [8] T. Skwarnicki, *A study of the radiative CASCADE transitions between the Upsilon-Prime*
560 *and Upsilon resonances*. PhD thesis, Cracow, INP, 1986.
561 [9] H. Albrecht et al., ARGUS, *Search for Hadronic $b \rightarrow u$ Decays*, Phys. Lett. B **241** (1990)
562 278–282.
563 [10] B. Grinstein and A. Kobach, *Model-Independent Extraction of $|V_{cb}|$ from $\bar{B} \rightarrow D^* \ell \bar{\nu}$* , Phys.
564 Lett. B **771** (2017) 359–364, arXiv:1703.08170 [hep-ph].
565 [11] D. Bigi, P. Gambino, and S. Schacht, *A fresh look at the determination of $|V_{cb}|$ from*
566 *$B \rightarrow D^* \ell \nu$* , Phys. Lett. B **769** (2017) 441–445, arXiv:1703.06124 [hep-ph].

Sig. Prob. > 0.001			
Channel	$N_{X\ell\nu}^{\text{MC}}$	$N_{X\ell\nu}^{\text{Data}}$	ϵ
$B^+ e^-$	$(4.46 \pm 0.11) \times 10^4$	$(2.94 \pm 0.08) \times 10^4$	0.66 ± 0.02
$B^+ \mu^-$	$(4.78 \pm 0.11) \times 10^4$	$(3.10 \pm 0.10) \times 10^4$	0.65 ± 0.03
$B^0 e^-$	$(1.75 \pm 0.04) \times 10^4$	$(1.46 \pm 0.07) \times 10^4$	0.83 ± 0.04
$B^0 \mu^-$	$(1.85 \pm 0.06) \times 10^4$	$(1.54 \pm 0.05) \times 10^4$	0.83 ± 0.04
Sig. Prob. > 0.01			
Channel	$N_{X\ell\nu}^{\text{MC}}$	$N_{X\ell\nu}^{\text{Data}}$	ϵ
$B^+ e^-$	$(2.65 \pm 0.07) \times 10^4$	$(1.63 \pm 0.05) \times 10^4$	0.62 ± 0.02
$B^+ \mu^-$	$(2.88 \pm 0.09) \times 10^4$	$(1.71 \pm 0.05) \times 10^4$	0.59 ± 0.03
$B^0 e^-$	$(1.11 \pm 0.03) \times 10^4$	$(0.84 \pm 0.04) \times 10^4$	0.76 ± 0.04
$B^0 \mu^-$	$(1.18 \pm 0.04) \times 10^4$	$(0.94 \pm 0.03) \times 10^4$	0.80 ± 0.04
Sig. Prob. > 0.1			
Channel	$N_{X\ell\nu}^{\text{MC}}$	$N_{X\ell\nu}^{\text{Data}}$	ϵ
$B^+ e^-$	$(1.10 \pm 0.03) \times 10^4$	$(0.71 \pm 0.03) \times 10^4$	0.65 ± 0.03
$B^+ \mu^-$	$(1.21 \pm 0.04) \times 10^4$	$(0.78 \pm 0.04) \times 10^4$	0.64 ± 0.03
$B^0 e^-$	$(0.60 \pm 0.02) \times 10^4$	$(0.43 \pm 0.02) \times 10^4$	0.72 ± 0.04
$B^0 \mu^-$	$(0.64 \pm 0.02) \times 10^4$	$(0.46 \pm 0.02) \times 10^4$	0.72 ± 0.04

TABLE III. Results for $N_{X\ell\nu}$ as determined from the fits to data and simulation together with total uncertainties. The corresponding calibration factors computed from the ratio of these yields are also shown for each channel.

567 [12] A. Abdesselam et al., Belle II Collaboration, *A fresh look at the determination of $|V_{cb}|$ from*
568 *$B \rightarrow D^* \ell \nu$* , arXiv:1702.01521 [hep-ph].

569 Appendix A: Appendix A

570 A summary of all fitted yields, $N_{X\ell\nu}^{\text{Data}}$, MC expected yields, $N_{X\ell\nu}^{\text{MC}}$ and the corresponding
571 calibration factors are provided in Table III.